Fast Patchwise Nonlocal SAR Image Despeckling Using Joint Intensity and Structure Measures

Dongxing Liang ⓘ, Ming Jiang, and Jinshan Ding ⓘ, *Member, IEEE*

Abstract—**Nonlocal means synthetic aperture radar (SAR) image despeckling approaches have attracted much research attention. However, high computational burden always limits its application in practice, especially using complex similarity measures. We present a fast patchwise nonlocal method using joint intensity and structure measures for SAR image despeckling. Nonlocal methods often define the similarity criterion only based on amplitude or intensity image. In order to preserve structure details, the structure information is also introduced into similarity measure by constructing gradient orientation feature map. The gradient orientation statistical test is performed to determine whether the patches contain the same structural components, and the similar patches are selected through the constant false alarm ratio strategy. Furthermore, we reorganize the patchwise nonlocal despeckling method and accelerate it using fast Fourier transform. Meanwhile, we utilize a Gaussian kernel to aggregate patchwise weights for each pixel in its patch area, so as to reduce the blur effect of classical patchwise nonlocal methods on details. The experiments have demonstrated that the proposed method is an efficient restoration method and has great structure and texture retention ability.**

Index Terms—**Despeckling, fast nonlocal means, gradient orientation, radar image, structure measure, synthetic aperture radar (SAR).**

I. INTRODUCTION

SYNTHETIC aperture radar (SAR) images have been widely used in remote sensing (RS) [1], [2]. However, SAR images are often difficult to interpret due to speckle noise caused by random constructive and destructive interference within a resolution cell. The speckle noise degrades SAR image quality, therefore impairing the performance of SAR image-based applications.

It is highly desired to recover clean images from noisy images, known as SAR image despeckling. Many SAR image despeckling approaches have been developed in the past decades. They can be categorized into the spatial domain-based methods [3]–[5] and the transformed domain-based methods [6]–[8], utilizing sparse representation models [9], [10] or variational models [11]–[13]. Recently, deep learning-based despeckling methods have received much attention, which mostly require supervision in training using simulated data or multilook images as the ground truth [14]–[18]. A self-supervised despeckling

method was proposed in [19]. The most successful despeckling approach so far has been the nonlocal paradigm [20], which has inaugurated a new generation of despeckling filters.

The nonlocal approaches, known as nonlocal means (NLM), was originally proposed in [21] for image denoising, which are based on the selfsimilarity property within image. The estimation of a pixel is performed by averaging similar pixels within the image (usually, within a search window for simplicity and faster computation). The key procedure of these approaches is the similarity measure, which is evaluated not directly on a considered pixel but on the patches centered on the considered pixel [22]. Over the last decade, several methods for measuring patch similarity have been proposed [23]–[25].

Since the nonlocal approach was applied to SAR [26], a few works have been reported with specific characteristics in terms of the adopted similarity criterion and/or the procedure used to fuse similar pixels. Under the assumption of additive white Gaussian noise, the sum of squared differences is regarded as an intuitive criterion for similarity evaluation between two patches. However, considering the characteristics of the multiplicative noise and non-Gaussian noise, specific criteria for SAR images must be derived. The criterion, adopted in [26], is the logarithm of the ratio between arithmetic and geometric means. Similar expressions were also reported in [27]–[29]. A direct amplitude ratio-based metric was proposed in [30], and the sigma filter was incorporated in the nonlocal framework [31]. In SAR-BM3D [32], the nonlocal and wavelet decomposition are combined to achieve satisfying results. Recently, a guided nonlocal filter was reported, combining SAR data and optical data to compute the joint filter weights, which requires strict coregistered SAR and optical images [33]. Most of these methods rely on strict speckle noise model assumption, while the assumption cannot be verified in some cases. Hence, a model-free nonlocal approach was proposed with two similarity criteria, one of which is obtained by directly comparing the distributions of the patches whereas the other compares the distribution of ratio patches [34].

It should be noted that the improvement in despeckling is achieved at the expense of high computation burden, which limits the applications of nonlocal approaches. Several methods have been proposed to reduce the computational cost. For instance, the method of preselection of pixels [35], early termination to eliminate dissimilar blocks [36] and multiresolution decomposition-based method [37], aim at reducing the number of similar pixels involved in calculation. Besides, the complexity of weight calculation can be decreased by using fast Fourier transform(FFT)-based operation [38], which is an alternative to

reduce the computational cost. FANS [39] employs a varying-size search area driven by the activity level of each patch to reduce the complexity, while probabilistic early termination and lookup table strategies are also used. However, most of these accelerated methods do not implement the exact nonlocal approaches, which may impair the denoised image quality.

We propose a computational efficient patchwise nonlocal approach for SAR image despeckling in this article. First, intensity and structure information are both considered in the similarity measure, where the structure information is represented by constructing the gradient orientation map. Meanwhile, we explore the statistical characteristics of gradient orientations, then the constant false alarm ratio (CFAR) strategy is employed to reject patches without obviously similar or with opposite structural components. In addition, we optimize the patchwise nonlocal algorithm so that it is accelerated by FFT. Finally, to tackle the blur influence in the conventional patchwise nonlocal despeckling, the filter weights derived from joint intensity and structure similarity measures are computed by aggregating all the patchwise weights within the patch area of each pixel using a Gaussian kernel.

This article is organized as follows. Section II briefly reviews the nonlocal approaches for SAR image despeckling. Section III describes the proposed method using joint weights combining the intensity and structure information and its acceleration by FFT in detail. Experimental results are shown in Section IV. Finally, Section V concludes this article.

II. NONLOCAL APPROACH

Assume a noisy image $\mathbf{V}$, $v(\mathbf{x}) = f(u(\mathbf{x}))$, where $v(\mathbf{x})$ and $u(\mathbf{x})$ denote, respectively, the degraded and true intensity values at coordinates $\mathbf{x} = (x_1, x_2)$, and $f(\cdot)$ denotes a degradation function. According to the nonlocal approach, the estimated value $\hat{u}(\mathbf{x})$ is computed as the weighted average of similar pixels $v(\mathbf{x} + \mathbf{t})$ within a search neighborhood $\mathbf{N_x}$ of $\mathbf{x}$

$$\hat{u}(\mathbf{x}) = \sum_{(\mathbf{x}+\mathbf{t})\in\mathbf{N_x}} w(\mathbf{x} + \mathbf{t}, \mathbf{x})v(\mathbf{x} + \mathbf{t}) \quad (1)$$

where $\mathbf{t} = (t_1, t_2)$ means a 2-D offset away from $\mathbf{x}$. The weight reflects the similarity level between the predictor patch $\mathbf{P}(\mathbf{x} + \mathbf{t})$ and the target patch $\mathbf{P}(\mathbf{x})$. Actually, based on the similarity, $\mathbf{P}(\mathbf{x} + \mathbf{t})$ can be either soft assigned or hard assigned to the set of similar patches of $\mathbf{P}(\mathbf{x})$ [20]. In the case of soft assignment, a weight reflecting the similarity level is associated to each patch within the search area; otherwise, if the patch $\mathbf{P}(\mathbf{x} + \mathbf{t})$ is significantly dissimilar to $\mathbf{P}(\mathbf{x})$, the pixel at $(\mathbf{x} + \mathbf{t})$ is simply removed from the neighborhood $\mathbf{N_x}$ or, equivalently, the weight $w(\mathbf{x} + \mathbf{t}, \mathbf{x})$ is set to 0.

Recently, patchwise NLM has been shown to significantly outperform the pixelwise version [20]. The main idea is to aggregate more estimates of the same pixel, which are eventually combined to reduce the estimate variance. In practice, this is achieved by computing the nonlocal weighted average of all the pixels of the target patch instead of only the center pixel, which

Algorithm 1: The Process of Classical Patchwise NLM.

Input: noisy image $\mathbf{V}$, half-length of patch size d_s, half-length of search window size D_s, interval S_d
Initialize: $\mathbf{V}_d \leftarrow$ array filled with 0
Output: denoised image $\mathbf{V}_d$
1: **for all** pixels at coordinates $\mathbf{x}$ in $\mathbf{V}$ with two dimensional intervals (S_d, S_d) **do**
2:      **for all** pixels at coordinates $(\mathbf{x} + \mathbf{t}) \in \mathbf{N_x}$ **do**
3:          Select the patches $\mathbf{P}(\mathbf{x})$ and $\mathbf{P}(\mathbf{x} + \mathbf{t})$
4:          Compute the weight $w(\mathbf{x} + \mathbf{t}, \mathbf{x})$
5:          Add $\mathbf{P}(\mathbf{x} + \mathbf{t})$ to the patch of coordinates $\mathbf{x}$ in $\mathbf{V}_d$ with weight $w(\mathbf{x} + \mathbf{t}, \mathbf{x})$
6:      **end for**
7: **end for**
8: Compute final estimate $\mathbf{V}_d$ with weights normalization

can be shown as follows:

$$\hat{u}(\mathbf{x} + \mathbf{k}) = \sum_{(\mathbf{x}+\mathbf{t})\in\mathbf{N_x}} w(\mathbf{x} + \mathbf{t}, \mathbf{x})v(\mathbf{x} + \mathbf{t} + \mathbf{k}) \quad \forall \mathbf{k} \in \mathbb{P}$$

$$(2)$$

where $\mathbb{P}$ indicates the set of spatial offsets with respect to the center point. It can be observed that a whole patch area can be denoised at the same time. Therefore, a 2-D interval can be used when the previous denoising process traverses the image, as long as the interval is smaller than the patch size. The algorithm of patchwise NLM is summarized in Algorithm 1.

Although the patchwise version was first presented as a way to reduce the complexity of pixelwise NLM using the 2-D interval [21], it is obvious that using fewer blocks in the aggregation procedure probably also reduce the denoising performance.

III. PROPOSED APPROACH FOR SAR DESPECKLING

In this section, we propose a computational efficient patchwise nonlocal approach using joint weights combining the intensity and structure information. The joint filtering weights provide more reliable predictors and reduce the dependence to the exact model of speckle noise. We reorganize the flowchart of the patchwise nonlocal and accelerate it through FFT.

A. Intensity Distance

Let us consider a common multiplicative model, $v(\mathbf{x}) = u(\mathbf{x})n(\mathbf{x})$, with $n(\mathbf{x})$ a gamma random variable modeling the speckle. The SAR intensity distance is computed with the ratio between the arithmetic and the geometric means

$$d_i[\mathbf{x} + \mathbf{t}, \mathbf{x}] = \frac{1}{N} \sum_{\mathbf{k}\in\mathbb{P}} \log\left[\frac{v(\mathbf{x} + \mathbf{t} + \mathbf{k}) + v(\mathbf{x} + \mathbf{k})}{2\sqrt{v(\mathbf{x} + \mathbf{t} + \mathbf{k})v(\mathbf{x} + \mathbf{k})}}\right] \quad (3)$$

where $N = |\mathbb{P}|$ is the patch size. This is the distance utilized in [28], which is considered as the generalized likelihood ratio and performs best. Specific statistical analysis is presented in [33].
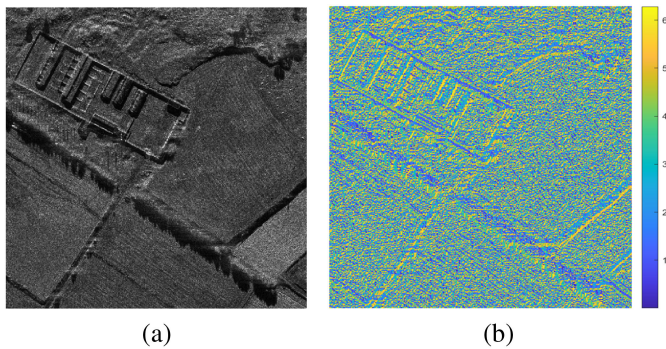
Fig. 1. Original SAR image and corresponding gradient orientation feature map (rad). (a) SAR image. (b) Gradient orientation map.

B. Structure Distance

To preserve the structure details, the structure similarity is measured in this article. The gradient orientation has been proved to be able to measure the structure similarity between RS images, even for multisource RS images [40]. Hence, we attempt to extract gradient orientation from an amplitude image as a feature map to be measured. Fig. 1 shows an original SAR image and the corresponding gradient orientation feature map, in which the gradient information is obtained by using Sobel operator. One can see that although the SAR image suffers from speckle noise, its structure and texture information can still be clearly observed in the corresponding gradient orientation map, which provides a basis for the subsequent use of gradient direction for structure similarity measure.

Inspired by Liang et al. [40], the patchwise structure measure is written as follows:

$$d_o[\mathbf{x} + \mathbf{t}, \mathbf{x}] = \frac{1}{N} \sum_{\mathbf{k} \in \mathbb{P}} \cos(o(\mathbf{x} + \mathbf{t} + \mathbf{k}) - o(\mathbf{x} + \mathbf{k})) \quad (4)$$

where $o(\mathbf{x} + \mathbf{t})$ and $o(\mathbf{x})$ represent the gradient orientation at coordinates $(\mathbf{x} + \mathbf{t})$ and $\mathbf{x}$, respectively. The distance is not exactly the same as the one with extra coefficient 2 in $\cos(\cdot)$ proposed in [40], because the gradient direction here belongs to $[0, 2\pi)$ instead of $[0, \pi)$ for multisource RS images.

Based on the structure measure, we would like to identify whether predictor patches have similar structural components as the target patch. Assuming that if a homogeneous region is full of random noise, its corresponding gradient orientation follows a uniform distribution $U(0, 2\pi)$ and is independent of the noise model. Common noise models, such as Gaussian, Rayleigh, and square root gamma distributions, are simulated, and the gradient direction distribution corresponding to each case is shown in Fig. 2. It can be clearly observed that the gradient orientation distribution always follows the uniform distribution $U(0, 2\pi)$ and is independent of the specific noise models, which is consistent with our hypothesis.

Further, let us consider the following three cases of patches:
1) flat patch,
2) patch with significant structure information, and
3) patch with different structure information from (2), and in extreme cases with opposite gradient directions.
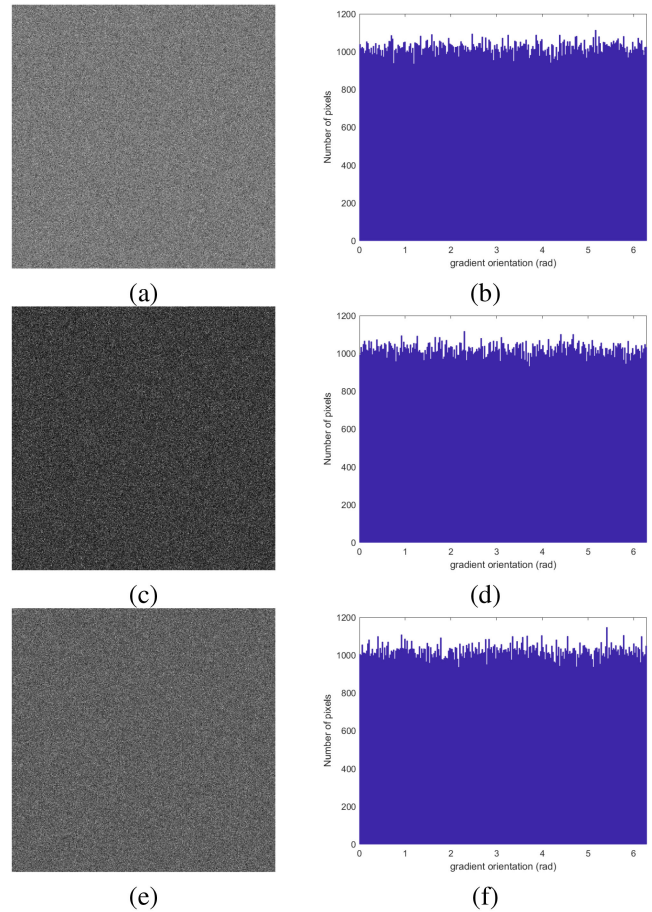

Fig. 2. Different noise models in amplitudes of SAR image and the corresponding gradient orientation distributions. (a) Gaussian noise. (b) Gradient orientation distribution of (a). (c) Rayleigh noise in the case of 1-look. (d) Gradient orientation distribution of (c). (e) Square root gamma noise in the case of 4-look. (f) Gradient distribution map of (e).

As expressed in (4), the difference of two orientations is presented such that

$$\Delta\theta = o_1 - o_2 \quad (5)$$

where o_1 and o_2, respectively, represent the gradient orientation values of the two pixels within two patches. It is intuitive that as long as one of the patches is a flat area, $\Delta\theta$ still obeys the uniform distribution $U(0, 2\pi)$. Hence, the structure similarity measure has no judgement for flat patches. If the two patches have a similar structure, the value of $\cos(\Delta\theta)$ will be close to 1; otherwise, the value will be close to -1 for patches with gradient inversion. Therefore, the similarity measure can help us to identify the patches with similar or opposite structural components. On this basis, the structure distance can be incorporated with intensity distance to provide more reliable predictors by improving the weights of patches with the same structure and suppressing the weights of patches with heterogeneous structures.

For a more precise analysis, the statistics of patchwise structure distance are supposed to be reported. As abovementioned, the adjacent pixels within 3×3 area are utilized in Sobel operation to compute the gradient information of the center pixel. Consequently, the gradient orientation variables in a patch
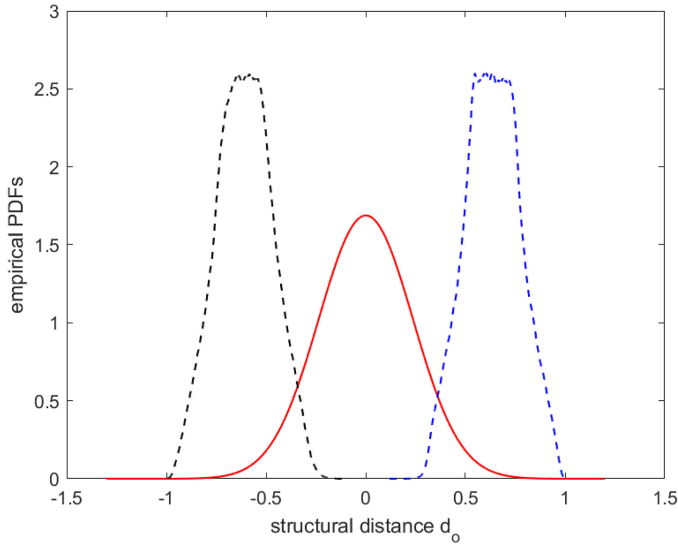
Fig. 3. Empirical PDFs of d_o for different cases. (1) One of patches is flat patch (solid red). (2) Patches with similar structural components (dashed blue). (3) Patches with opposite structural components (dashed black).
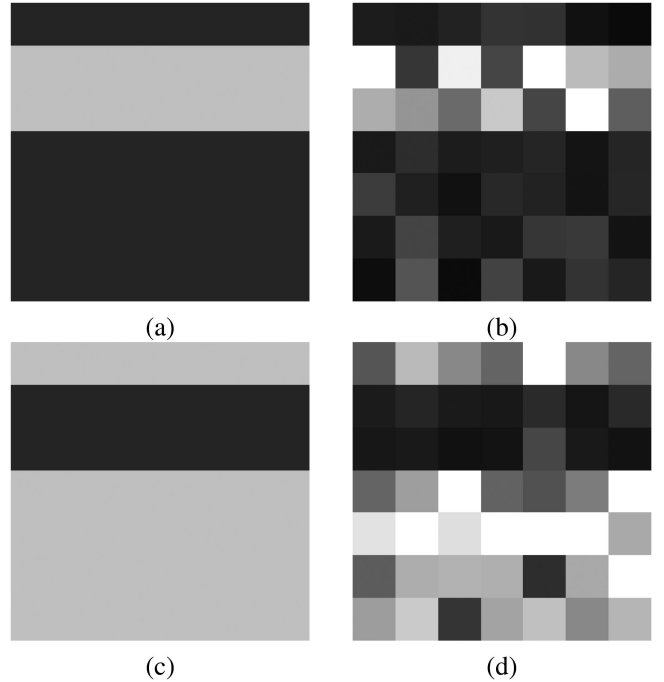

Fig. 4. Original SAR patches and the corresponding noisy patches. (a) Reference SAR patch. (b) Noisy version of (a). (c) SAR patch with opposite structure. (d) Noisy version of (c).

violate the independence. For the convenience of subsequent statistical analysis, the structure distance is rewritten as follows:

$$
d_o[\mathbf{x} + \mathbf{t}, \mathbf{x}]
$$
$$
= \frac{1}{N'} \sum_{\{\mathbf{k} \in \mathbb{Z}^2 : |3\mathbf{k}|_\infty \leq d_s\}} \cos(o(\mathbf{x} + \mathbf{t} + 3\mathbf{k}) - o(\mathbf{x} + 3\mathbf{k})) \quad (6)
$$

where N' presents the actual number of pixels involved in the measure. By selecting the center pixel for each 3×3 region, the selected gradient orientations follows independent identically uniform distribution $U(0, 2\pi)$. Given an example, assuming a patch of gradient orientation map with size of 7×7, the mask to select pixels is presented as follows:

$$
M_o = \frac{1}{9}
\begin{bmatrix}
1 & 0 & 0 & 1 & 0 & 0 & 1 \\
0 & 0 & 0 & 0 & 0 & 0 & 0 \\
0 & 0 & 0 & 0 & 0 & 0 & 0 \\
1 & 0 & 0 & 1 & 0 & 0 & 1 \\
0 & 0 & 0 & 0 & 0 & 0 & 0 \\
0 & 0 & 0 & 0 & 0 & 0 & 0 \\
1 & 0 & 0 & 1 & 0 & 0 & 1
\end{bmatrix} \quad (7)
$$

where the nonzero numbers represent the active ($N' = 9$ in this case) pixels in the patch contributing to the structure distance in this case. For the case $\Delta\theta \sim U(0, 2\pi)$, $\cos(\Delta\theta)$ is a random variable with zero mean and variance of $1/2$. The patchwise structure distance $d_o[x + t, x]$ is the sum of N' independent identically distributed random variables, which can be well approximated by a Gaussian law with zero mean and variance σ^2 of $1/(2 N')$. Note that the statistics are independent to the noise model. In order to verify the theoretical analysis, we resort to Monte Carlo simulation. Fig. 3 plots the empirical probability density function (PDF) of structure distance between two flat patches (solid red).

Then, two patches with the same gradient orientations or opposite gradient orientations are considered. Fig. 4 presents the noise-free patches and corresponding noisy versions.

Lacking the closed form of the PDFs, we still resort to Monte Carlo simulation. Fig. 3 illustrates the empirical PDFs for two patches with the same structure (dashed blue) and for two patches with opposite gradient information (dashed black). As expected, the PDFs with significant structure can be well separated. Therefore, the CFAR strategy is adopted to select patches with strong structure information. Specifically, we set a threshold T and assign the structure distance less than T to zero such that

$$
d_o(\mathbf{x} + \mathbf{t}, \mathbf{x}) =
\begin{cases}
0 & |d_o(\mathbf{x} + \mathbf{t}, \mathbf{x})| \leq T \\
d_o(\mathbf{x} + \mathbf{t}, \mathbf{x}) & |d_o(\mathbf{x} + \mathbf{t}, \mathbf{x})| > T.
\end{cases} \quad (8)
$$

C. Joint Intensity and Structure Weight

Obtaining the patchwise intensity and structure distances, the joint weight needs to be further determined. First, the intensity weight is simply defined as follows:

$$
w_i(\mathbf{x} + \mathbf{t}, \mathbf{x}) = C_i \exp\{-\lambda d_i(\mathbf{x} + \mathbf{t}, \mathbf{x})\} \quad (9)
$$

where C_i is a normalization constant and λ determines the decay of the exponential function.

As for the structure weight, the structure distance can only judge whether two patches have similar structure or different structure except for flat patches, as analyzed in the previous section. As long as two patches have the same gradient orientation information, the high similarity score will be obtained regardless of the intensity difference between them. Hence, the structure weight can be only taken as a gain of the intensity
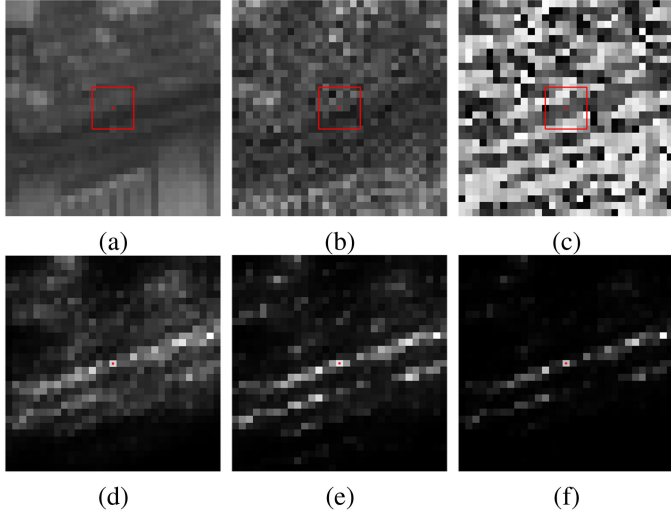
(a) (b) (c)

(d) (e) (f)

Fig. 5. Images to show the effect of joint weight. The center pixel and patch are highlighted in red. (a) Original image window. (b) Noisy image window. (c)Gradient orientation map of (b). (d) Weight map computed according to (9). (e) Gain map from (10). (f) Joint weight map from (11).

weight, and the intensity distance is supposed to be taken into account to calculate the gain at the same time. The gain is defined as follows:

$$g_o(\mathbf{x} + \mathbf{t}, \mathbf{x}) = C_o \exp\{-\lambda d_i(\mathbf{x} + \mathbf{t}, \mathbf{x})[1 - d_o(\mathbf{x} + \mathbf{t}, \mathbf{x})]\} \tag{10}$$

where C_o is a normalization constant. The expression brings a high gain if there is a high similarity in both intensity and structure, or a low gain if one of them is weak.

Combining (9) and (10), the final joint weight is expressed as follows:

$$\begin{aligned} w(\mathbf{x} + \mathbf{t}, \mathbf{x}) &= w_i(\mathbf{x} + \mathbf{t}, \mathbf{x})g_o(\mathbf{x} + \mathbf{t}, \mathbf{x}) \\ &= C \exp\{-\lambda d_i(\mathbf{x} + \mathbf{t}, \mathbf{x})[2 - d_o(\mathbf{x} + \mathbf{t}, \mathbf{x})]\} \end{aligned} \tag{11}$$

where C is the joint normalization constant.

Fig. 5 shows an example of introducing gradient orientation into weight calculation. As shown in the original image window, the target patch includes only a small effective number of similar patches, which are along the edge. The pixel intensity difference in the noisy image is not obvious, which makes it unreliable to select the similar patches only by intensity. Fig. 5(d) presents the intensity weight map, where some dissimilar patches are also assigned with high weights. Although the image intensity information is destroyed to some extent, some structure information can still be clearly observed in the gradient orientation map, as shown in Fig. 5(c). The corresponding gain map and the joint weight map are presented in Fig. 5(e) and (f). As we can see, the weights of unreliable patches are suppressed in the joint weight map, which verify the effectiveness of using gradient direction information.

D. Fast Patchwise NLM

In this section, a fast nonlocal flowchart is introduced. As described in Algorithm 1, the target patch is estimated simultaneously. A noticeable fact is that the pixelwise similarity measure is repeatedly calculated in the classical patchwise nonlocal methods, and the larger the patch size, the more time-consuming the repeated calculation. Therefore, first, loops are rearranged so that one considers all pixels $\mathbf{x}$ for all translation vectors $\mathbf{t} \in [-D_s, +D_s]^2$. Then, given such a $\mathbf{t}$, the distance maps of intensity and structure are, respectively, obtained as follows:

$$s_i(\mathbf{x}, \mathbf{t}) = \log \left\{ \frac{v(\mathbf{x}) + v(\mathbf{x} + \mathbf{t})}{2\sqrt{v(\mathbf{x})v(\mathbf{x} + \mathbf{t})}} \right\} \tag{12a}$$

$$s_o(\mathbf{x}, \mathbf{t}) = \cos(o(\mathbf{x}) - o(\mathbf{x} + \mathbf{t})). \tag{12b}$$

The corresponding weighted norms of patch differences are written as a discrete convolution product

$$\begin{aligned} d_i(\mathbf{x}, \mathbf{x} + \mathbf{t}) &= \sum_{\{\mathbf{k} \in \mathbb{Z}^2 : \|\mathbf{k}\|_\infty \le d_s\}} K_i(\mathbf{k})s_i(\mathbf{x} + \mathbf{k}, \mathbf{t}) \\ &= (\tilde{K}_i * s_i(\mathbf{t}))(\mathbf{x}) \end{aligned} \tag{13a}$$

$$\begin{aligned} d_o(\mathbf{x}, \mathbf{x} + \mathbf{t}) &= \sum_{\{\mathbf{k} \in \mathbb{Z}^2 : \|\mathbf{k}\|_\infty \le d_s\}} K_o(\mathbf{k})s_o(\mathbf{x} + \mathbf{k}, \mathbf{t}) \\ &= (\tilde{K}_o * s_o(\mathbf{t}))(\mathbf{x}) \end{aligned} \tag{13b}$$

where $\tilde{K}_i(\mathbf{k}) = K_i(-\mathbf{k})$ and $\tilde{K}_o(\mathbf{k}) = K_o(-\mathbf{k})$ demonstrate the weighted kernels for intensity and structure relatively, the operator $*$ represents the discrete convolution production, and $s_i(\mathbf{t})$ and $s_o(\mathbf{t})$ indicate intensity and structure distance map corresponding to the shift vector $\mathbf{t}$. It is worth noting that the kernels used in intensity and structure measures are different. The kernel for intensity is a $(2d_s + 1) \times (2d_s + 1)$ normalized matrix with the same elements, while a matrix with the form such as M_o for structure. After obtaining these patchwise distances, the joint weights can be computed according to (11).

In this way, the repeated pixelwise distance calculation is eliminated, and then, how to efficiently realize (2) needs our further consideration.

The target pixel belongs to an amount of patches, not only the patch centered on it. The weights between a considered pixel and the target pixel are not only related on the similarity measures between two patches center on them, but also all corresponding patches including the two pixels. Fig. 6 shows a simple example to illustrate this issue. There are two pixels v_1 and v_2 with given offset $\mathbf{t}_1$. The estimation of pixel v_1 does not only rely on the weight measured by the two red patches centered on them to weighted average the value of v_2, but also the weights measured by two green patches, two blue patches and other corresponding patches including the two pixels. Actually, these weights between v_1 and v_2 are exactly the weights obtained between each patch centered on the point in the patch area of v_1 and the corresponding patch with the same $\mathbf{t}_1$.
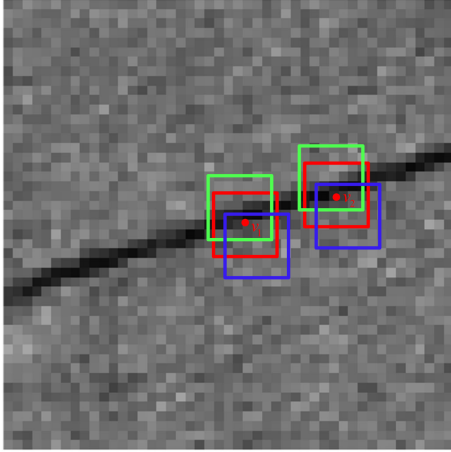
Fig. 6. Representation of patchwise approach: the considered pixel is weighted average with different weights measured by all corresponding patches including the considered and the target pixels, but not only patches centered on them.

Hence, the weighted average procedure can be rewritten as follows:

$$\hat{u}(\mathbf{x}) = \sum_{\mathbf{t} \in [-D_s, D_s]^2} \sum_{\mathbf{m} \in [-d_s, d_s]^2} w(\mathbf{x} + \mathbf{m}, \mathbf{x} + \mathbf{m} + \mathbf{t}) v(\mathbf{x} + \mathbf{t})$$

$$= \sum_{\mathbf{t} \in [-D_s, D_s]^2} (K_p * w)(\mathbf{x} + \mathbf{t}) v(\mathbf{x} + \mathbf{t}) \quad (14)$$

where K_p is a normalized kernel with the same elements to collect the patchwise weights within a patch area.

As it is well known, the convolution operation can be accelerated by using 2D-FFT denoted by $\mathcal{F}$ and its inverse $\mathcal{F}^{-1}$

$$\tilde{K} * s_i = \mathcal{F}^{-1}(\mathcal{F}(\tilde{K}) \mathcal{F}(s_i)). \quad (15)$$

Thus, all convolution operations mentioned above are accelerated using the same means as (15).

Although patchwise nonlocal filter has been proved to be effective in reducing the rare patch effect [20], we found that the details will be blurred and several structure contours are eroded so that some small targets disappear. To conduct an in-depth analysis of this issue, let us consider a special case of a pixel near a line, such as the red point shown in Fig. 7(a), where the rectangles represent patches with the size of 7×7. It is clear that the patch centered on the target pixel has strong heterogeneity and most other patches, due to the homogeneous area in the search region, are obviously dissimilar from it. Using pixelwise nonlocal filter, only a small effective number of patches, dashed red ones along the black gap in Fig. 7(a), can be utilized to the average, which results in high variance. As a result, a visible "halo" of residual noise is observed near the gap, as shown in Fig. 7(b). However, the target pixel belongs to a large number of patches centered on the neighboring pixels of the target pixel and these neighboring pixels are within the patch area of the target pixel. In the patchwise NLM, all of these patches are included in the average reducing the estimate variance. However, many pseudo similar patches, such as the green rectangles with high weights, may be included in the procedure in Fig. 7(a). The solid green patch contains the target pixel at the corner of the patch,

---

Algorithm 2: The Process of FND-IS Algorithm.

Input: noisy image $\mathbf{V}$, half-length of patch size d_s, half-length of search window size D_s, threshold T

Initialize: $\mathbf{V}_{sym} \leftarrow$ symmetrized noisy image
$\mathbf{V}_d \leftarrow$ array filled with 0

Output: denoised image $\mathbf{V}_d$

1: Construct gradient orientation map $\mathbf{G}$ and symmetrized version $\mathbf{G}_{sym}$
2: **for** $\mathbf{t} = (t_1, t_2) \in [-D_s, D_s]^2$ **do**
3:     Select the intensity map and gradient orientation map $\mathbf{V}_{sym}[\mathbf{t}]$ and $\mathbf{G}_{sym}[\mathbf{t}]$
4:     Compute the element-wise distance between $\mathbf{V}$ and $\mathbf{V}_{sym}[\mathbf{t}]$, $\mathbf{G}$ and $\mathbf{G}_{sym}[\mathbf{t}]$
5:     Compute the patchwise distance $\mathbf{d}_i(\mathbf{t})$ and $\mathbf{d}_o(\mathbf{t})$ using FFT
6:     Transform $\mathbf{d}_o(\mathbf{t})$ according to (8)
7:     Compute the joint filtering weight map $\mathbf{w}(\mathbf{t})$ according to (11)
8:     Collect all patchwise weights within the patch area for each pixel according to (15)
9:     Add the $\mathbf{V}_{sym}[\mathbf{t}]$ to the $\mathbf{V}_d$ with corresponding weights
10: **end for**
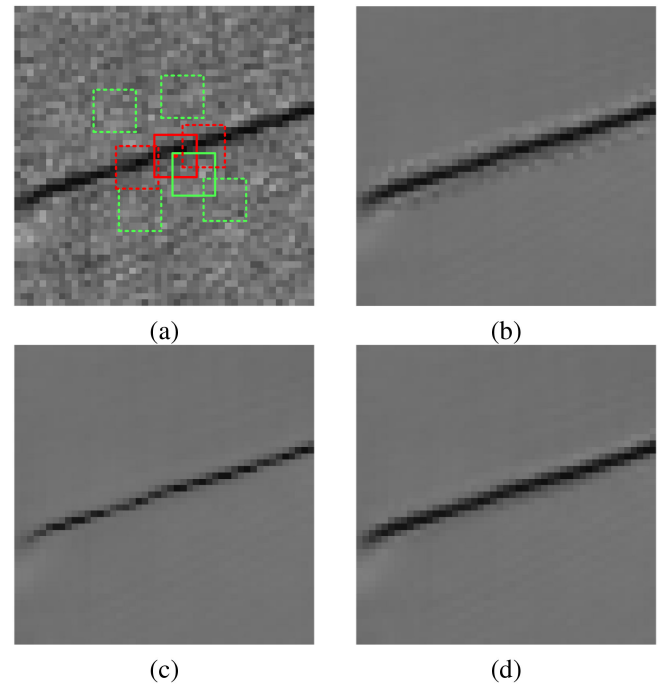
Fig. 7. Denoising results using different nonlocal filters. (a) Original noisy image. (b) Classical pixelwise nonlocal method. (c) Classical patchwise nonlocal method. (d) Proposed method with a Gaussian kernel.

which is strongly similar to other dashed green patches in the homogeneous region. Nevertheless, the target pixel is clearly different from the corresponding pixels in these pseudo similar patches and the number of these pseudo similar patches is much larger than the actual number of similar patches. In the classical

TABLE I
DETAIL INFORMATION OF THE TEST IMAGES

| Category	Image No.	Source	Frequency	Mode	Date	Location
Single-Look	No.1 [33]	TerraSAR-X	X	Spotlight	01/2008	Image covers suburban area with buildings
	No.2	TerraSAR-X	X	Stripmap	08/2016	Image covers urban area with buildings
	No.3	Gaofen-3	C	Spotlight	04/2011	Image covers urban area
	No.4	Airborne	W	Spotlight	12/2019	Image covers a crossroad
Multi-Look	No.5	Airborne	Ka	Stripmap	04/2021	Image covers urban area with buildings and farmland
	No.6	Airborne	Ka	Stripmap	04/2021	Image covers a factory
	No.7	Airborne	Ka	Stripmap	04/2021	Image covers a town area with buildings
	No.8	Airborne	Ka	Stripmap	04/2021	Image covers suburban area with buildings and farmland
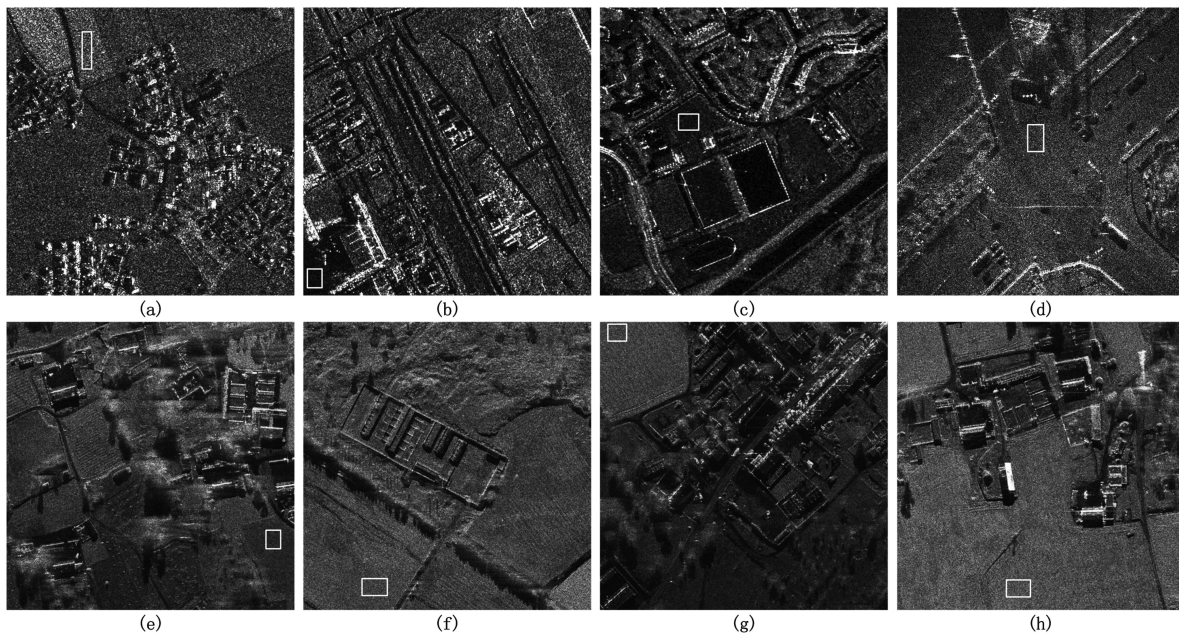
Fig. 8. Test images. (a) No.1. (b) No.2. (c) No.3. (d) No.4. (e) No.5. (f) No.6. (g) No.7. (h) No.8.

patchwise NLM, Fig. 7(c) shows the filtered result, where the black gap is significantly thinner and the edge details are blurred.

In order to deal with the issue, we would like to use a spatial kernel in (14), where K_p is set to a Gaussian kernel such that

$$\forall \mathbf{m} \in \mathbb{Z}, |\mathbf{m}|_\infty \leq d_s, K_p(\mathbf{m}) = \frac{e^{-\frac{|\mathbf{m}|^2}{2\sigma_1^2}}}{\sum_{\{\mathbf{j} \in \mathbb{Z}^2: |\mathbf{j}|_\infty \leq d_s\}} e^{-\frac{|\mathbf{j}|^2}{2\sigma_1^2}}} \quad (16)$$

where σ_1 controls the action range of Gaussian kernel, and the value is set to $d_s/3$ in the article. With the improvement, Fig. 7(d) presents the despeckling result in the proposed method. As we can see, the proposed method provides a satisfactory result, which outperforms the conventional pixelwise and patchwise NLM.

The proposed method, called as fast nonlocal despeckling, using joint intensity and structure measures (FND-IS), is described in Algorithm 2.

IV. EXPERIMENTAL RESULTS

A. Datasets

The experiments conducted on real SAR images are presented. Four single-look and four multilook SAR images were both tested to validate the effect of the proposed method. To evaluate the robustness of the proposed approach, the test images were acquired from different sensors, different platforms, different work frequency, and different work modes. These images cover a variety of scenes, such as urban, suburban, farmland, and crossroad. The detail information of the test images are presented in Table I, and all the images are shown in Fig. 8.

B. Key Parameters

The proposed method depends on several key parameters. In Algorithm 2, all key parameters are presented. Some of them were simply set similar to other literatures, such as search

window size, 21×21, and patch size, 7×7. With a low false alarm ratio, the threshold T was set to $1 + 2\sigma$, which is 1.47, as analyzed in Section III-B. The selection of T is independent of the noise model. The decay λ has a rather obvious meaning and need no more special analysis. A common principle is that for large noise, λ is supposed to be set a smaller value to smooth the image. On the contrary, for small noise variance, a larger value is preferred to preserve the image details. In the experiments, λ was set as 10 and 30 for single-look and multilook images, respectively.

C. Evaluation

A good filter is supposed to guarantee both effective reduction of speckle and reliable preservation of structure details, but these requirements are often contradictory. In general, deep despeckling tends to blur details of the image, while conservative details preserving leads to residual speckle remained in the image. Therefore, two quantitative criteria, equivalent number of looks (ENL) and edge-preservation degree-based ratio of average (EPD-ROA), to evaluate the image quality are considered. Besides, visual inspection is necessary to assess details of the filtered images.

ENL is the squared ratio between the mean and the standard deviation of the image intensity over a homogeneous region of the image. The regions utilized to compute the index are drawn in white boxes in Fig. 8. The ideal value should be as large as possible.

EPD-ROA [30] measures the quality of edge preservation in the filtered image, which is expressed as follows:

$$\text{EPD-ROA} = \frac{\sum_{j=1}^{n} |\hat{v}_{D_1}(j)/\hat{v}_{D_2}(j)|}{\sum_{j=1}^{n} |v_{o_1}(j)/v_{o_2}(j)|} \quad (17)$$

where n is the total number of selected regions, $\hat{v}_{D_1}(j)$ and $\hat{v}_{D_2}(j)$ represent two adjacent pixels of the filtered image in a certain direction (usually horizontal or vertical), and $v_{o_1}(j)$ and $v_{o_2}(j)$ are two pixels of the original image corresponding to $\hat{v}_{D_1}(j)$ and $\hat{v}_{D_2}(j)$. The closer EPD-ROA to 1, the better the edge preservation. In the subsequent experiments, the average of EPD-ROA obtained in the horizontal and vertical directions is computed.

Except for these indicators to measure the quality of the filtered images, the execution time of the despeckling method is also an important consideration for applications in practice.

D. Reference Methods

We compared the performance of the proposed method with the state-of-the-art methods, such as PPB, FANS, GNLMS, and MEET-SAR, with a brief summary given as follows.

1) *PPB* [26]*:* A probabilistic patch-based nonlocal filter, where the output is given by an iterative weighted maximum likelihood estimator.
2) *FANS* [39]*:* A faster and spatially adaptive version of SAR-BM3D [32], which is superior to the original SAR-BM3D.
3) *GNLMS* [33]*:* A guided patchwise nonlocal method using optical images is called GNLM, but it is also effective with only SAR images. In this section, GNLMS is derived

TABLE II
ENLs OF SINGLE-LOOK IMAGES

No.	noisy	PPB	FANS	GNLMS	MEET-SAR	FND-IS
1	1.04	**72**	62	27	38	47
2	0.99	**31**	24	16	11	23
3	1.12	**29**	16	22	16	27
4	1.06	**88**	73	53	31	79
Avg	1.05	**55**	43.75	29.5	24	44

Bold entities are used to indicate the best performance among the algorithms, as suggested by the Review Board.

TABLE III
ENLs OF MULTILOOK IMAGES

No.	noisy	PPB	FANS	GNLMS	MEET-SAR	FND-IS
5	3.46	177	118	157	102	**229**
6	3.91	352	317	251	320	**381**
7	3.48	**540**	324	283	349	526
8	4.01	**437**	229	211	277	383
Avg	3.72	376.5	247	225.5	262	**379.75**

Bold entities are used to indicate the best performance among the algorithms, as suggested by the Review Board.

from GNLM as only SAR images considered for a fair comparison.
4) *MEET-SAR* [34]*:* A model-free nonlocal denoising method, which is independent of the noise model.

For all of the reference methods, the suggested parameters in the original papers were retained. A noticeable fact is that there are some hidden parameters in these reference methods, such as the interval S_d described in Algorithm 1. All of the intervals were set to 1, which ensure the exact implementation of the approaches and make it faithful for comparison.

E. Performance Analysis

Tables II and III show the ENL results for single-look test images and multilook images, respectively. Table IV reports the average EPD-ROA values in horizontal and vertical directions.

The proposed method outperforms other reference methods in most cases. Especially for the multilook case, the proposed method provides the best results in both speckle reduction and details preservation. This may benefit from the improvement of signal-to-noise ratio (SNR) so as we can further smooth images while maintaining the structure details due to the gradient information. Among these methods, PPB provides competitive or even the best ENLs in single-look case to ensure effective speckle reduction, but some details are lost according to the values of EPD-ROA. FANS and GNLMS obtain similar results in speckle reduction and detail preservation, where the ENLs of FANS is slightly higher than GNLMS for single-look case. MEET-SAR seems to produce the least values in both ENL and EPD-ROA.
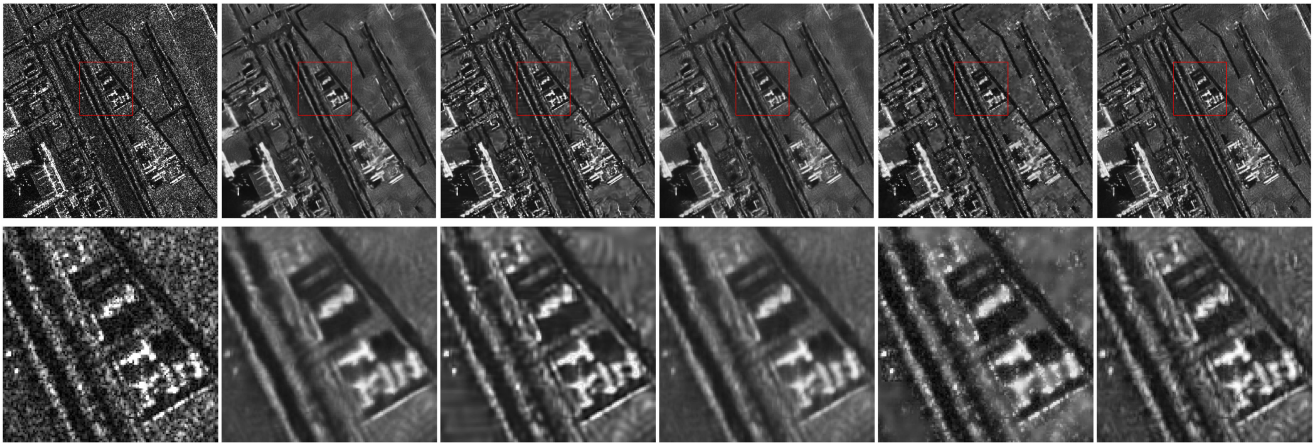
Fig. 9. Denoising results over a test single-look image. Row 1 (from left-hand side to right-hand side): original image, despeckling results of PPB, FANS, GNLMS, MEET-SAR, and proposed method, respectively. Row 2: excerpts from row 1 highlighted in red.
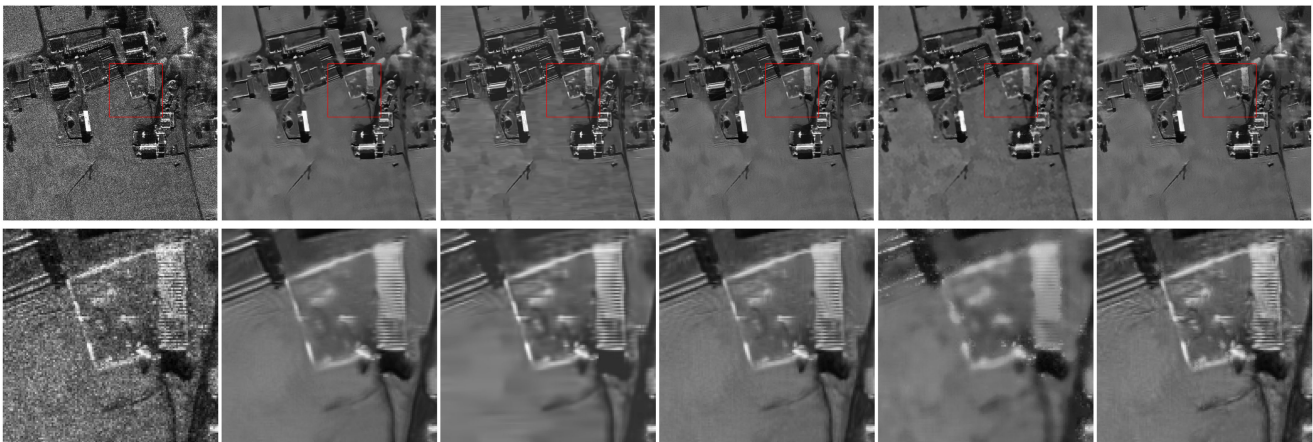

Fig. 10. Denoising results over a test multilook image. Row 1 (from left-hand side to right-hand side): original image, despeckling results of PPB, FANS, GNLMS, MEET-SAR, and proposed method, respectively. Row 2: excerpts from row 1 highlighted in red.

TABLE IV
EPD-ROA OF TEST IMAGES

No.	PPB	FANS	GNLMS	MEET-SAR	FND-IS
1	0.6873	0.6943	0.6890	**0.6972**	0.6950
2	0.7220	0.7340	0.7231	0.7362	**0.7384**
3	0.7691	0.7808	0.7714	0.7815	**0.7858**
4	0.6621	0.6644	0.6715	0.5432	**0.6736**
5	0.9452	0.9379	0.9511	0.9382	**0.9583**
6	0.9573	0.9546	0.9594	0.9568	**0.9654**
7	0.9280	0.9213	0.9269	0.9192	**0.9301**
8	0.9548	0.9590	0.9598	0.9478	**0.9600**
Avg	0.8282	0.8308	0.8315	0.8150	**0.8383**

Bold entities are used to indicate the best performance among the algorithms, as suggested by the Review Board.

To further compare the denoising details, Figs. 9 and 10 present filtered results and zoomed areas of a single-look sample and multilook sample, respectively. Through a visual comparison, PPB can effectively suppress speckle, but sometimes smear edges and structures such as buildings. Likewise, FANS also performs smoother results, but remarkable wavelet-related artifacts, which degrades the image quality. GNLMS provides better results in speckle suppression and detail preserving. However, on close inspection, some details are blurred and structure contours are eroded. MEET-SAR maintains the image details at the expense of poor speckle reduction for single-look case, but provides smoother result for multilook case. For both of single-look and multilook cases, the proposed method performs well in speckle reduction and structure preservation. Especially, with the improvement of the SNR of the SAR images, the proposed method outperforms the others, which smooths the homogeneous areas and retains the details.

F. Computational Cost

In this section, the computational cost of these methods is evaluated in terms of image size. The image size $l \times l$ is varying with $l = 64, 128, 256, 512, 1024$. The computational

TABLE V
RUN TIME (S)

Size l	64	128	256	512	1024
PPB	19.65	35.4	97	354.5	1283
FANS	0.15	0.53	2.6	11.2	41.2
GNLMS	25	119	438	1150	6171
MEET-SAR	192	1188	4813	21045	65532
FND-IS	**0.10**	**0.21**	**0.6**	**2.5**	**9.1**

Bold entities are used to indicate the best performance among the algorithms, as suggested by the Review Board.

complexity of the methods was evaluated by CPU time on a 3.40 GHz 64 b desktop equipped with 64 GB memory. The source code of PPB and FANS, based on C++ mex function, are available in [41] and [42], respectively, while the rest of the methods are implemented in MATLAB.

Table V reports the running time for the methods versus the various image size. We note that MEET-SAR is at least seven times more computationally expensive than the other methods, which is intractable in practical applications. This is because the distribution measure is time-consuming, and four anisotropic patch shapes are taken into account, which further increases the computational time of the method. GNLMS is the second only to MEET-SAR in the execution time, as it is implemented pixel by pixel in the spatial domain. PPB and FANS, due to the C++ implementation, are theoretically faster than the other methods implemented in MATLAB. Between FANS and PPB, FANS is at least 30 times faster than PPB as FANS uses varying size search area and lookup tables and employs a probabilistic early termination approach. Although implemented in MAT-LAB, our proposed method is the most efficient among all of the methods, noting three magnitudes faster than MEET-SAR, two magnitudes than PPB and GNLMS, and several times than FANS.

It has been demonstrated that the proposed method is the most efficient and provide competitive or even the best despeckling results.

V. CONCLUSION

An efficient patchwise nonlocal method based on joint intensity and structure measures has been proposed in this article for fast SAR image despeckling. We introduce the structure information into similarity measure that is independent of the noise model and the number of looks. Then, the CFAR strategy is adopted to ensure reliable similar patches. Meanwhile, the proposed method is accelerated by FFT after theoretical optimization. In addition, a Gaussian kernel is utilized to suppress the weights of some pseudo similar patches, which can avoid oversmoothed area and retain more details. The experimental results have convinced the efficiency of this method.

The gradient orientation information cannot be fully utilized due to the independence requirement, which can be further improved. Future work focuses on further exploring the statistical characteristics of structure features.

REFERENCES

[1] M. L. R. Sarker, J. Nichol, H. B. Iz, B. B. Ahmad, and A. A. Rahman, "Forest biomass estimation using texture measurements of high-resolution dual-polarization C-band SAR data," *IEEE Trans. Geosci. Remote Sens.*, vol. 51, no. 6, pp. 3371–3384, Jun. 2013.

[2] C. He, G.-S. Xia, and H. Sun, "An adaptive and iterative method of urban area extraction from SAR images," *IEEE Geosci. Remote Sens. Lett.*, vol. 3, no. 4, pp. 504–507, Oct. 2006.

[3] J.-S. Lee, "Digital image enhancement and noise filtering by use of local statistics," *IEEE Trans. Pattern Anal. Mach. Intell.*, vol. PAMI-2, no. 2, pp. 165–168, Mar. 1980.

[4] A. Lopes, R. Touzi, and E. Nezry, "Adaptive speckle filters and scene heterogeneity," *IEEE Trans. Geosci. Remote Sens.*, vol. 28, no. 6, pp. 992–1000, Nov. 1990.

[5] J.-S. Lee, J.-H. Wen, T. L. Ainsworth, K.-S. Chen, and A. J. Chen, "Improved sigma filter for speckle filtering of SAR imagery," *IEEE Trans. Geosci. Remote Sens.*, vol. 47, no. 1, pp. 202–213, Jan. 2009.

[6] F. Argenti and L. Alparone, "Speckle removal from SAR images in the undecimated wavelet domain," *IEEE Trans. Geosci. Remote Sens.*, vol. 40, no. 11, pp. 2363–2374, Nov. 2002.

[7] A. Achim, P. Tsakalides, and A. Bezerianos, "SAR image denoising via bayesian wavelet shrinkage based on heavy-tailed modeling," *IEEE Trans. Geosci. Remote Sens.*, vol. 41, no. 8, pp. 1773–1784, Aug. 2003.

[8] T. Bianchi, F. Argenti, and L. Alparone, "Segmentation-based MAP despeckling of SAR images in the undecimated wavelet domain," *IEEE Trans. Geosci. Remote Sens.*, vol. 46, no. 9, pp. 2728–2742, Sep. 2008.

[9] C. Ozcan, B. Sen, and F. Nar, "Sparsity-driven despeckling for SAR images," *IEEE Geosci. Remote Sens. Lett.*, vol. 13, no. 1, pp. 115–119, Jan. 2016.

[10] S. Tabti, L. Verdoliva, and G. Poggi, "Sparse-coding adapted to SAR images with an application to despeckling," in *Proc. IEEE Int. Geosci. Remote Sens. Symp.*, 2018, pp. 3695–3698.

[11] L. Denis, F. Tupin, J. Darbon, and M. Sigelle, "SAR image regularization with fast approximate discrete minimization," *IEEE Trans. Image Process.*, vol. 18, no. 7, pp. 1588–1600, Jul. 2009.

[12] W. Feng, H. Lei, and Y. Gao, "Speckle reduction via higher order total variation approach," *IEEE Trans. Image Process.*, vol. 23, no. 4, pp. 1831–1843, Apr. 2014.

[13] Y. Zhao, J. G. Liu, B. Zhang, W. Hong, and Y.-R. Wu, "Adaptive total variation regularization based SAR image despeckling and despeckling evaluation index," *IEEE Trans. Geosci. Remote Sens.*, vol. 53, no. 5, pp. 2765–2774, May 2015.

[14] G. Chierchia, D. Cozzolino, G. Poggi, and L. Verdoliva, "SAR image despeckling through convolutional neural networks," in *Proc. IEEE Int. Geosci. Remote Sens. Symp.*, 2017, pp. 5438–5441.

[15] P. Wang, H. Zhang, and V. M. Patel, "SAR image despeckling using a convolutional neural network," *IEEE Signal Process. Lett.*, vol. 24, no. 12, pp. 1763–1767, Dec. 2017.

[16] E. Dalsasso, X. Yang, L. Denis, F. Tupin, and W. Yang, "SAR image despeckling by deep neural networks: From a pretrained model to an end-to-end training strategy," *Remote Sens.*, vol. 12, 2020, Art. no. 2636.

[17] D. Cozzolino, L. Verdoliva, G. Scarpa, and G. Poggi, "Nonlocal CNN SAR image despeckling," *Remote Sens.*, vol. 12, no. 6, 2020, Art. no. 1006.

[18] A. Sebastianelli, M. P. Del Rosso, S. L. Ullo, and P. Gamba, "A speckle filter for Sentinel-1 SAR ground range detected data based on residual convolutional neural networks," *IEEE J. Sel. Topics Appl. Earth Observ. Remote Sens.*, vol. 15, pp. 5086–5101, 2022.

[19] A. B. Molini, D. Valsesia, G. Fracastoro, and E. Magli, "Speckle2Void: Deep self-supervised SAR despeckling with blind-spot convolutional neural networks," *IEEE Trans. Geosci. Remote Sens.*, vol. 60, 2021, Art. no. 5204017.

[20] C.-A. Deledalle, L. Denis, G. Poggi, F. Tupin, and L. Verdoliva, "Exploiting patch similarity for SAR image processing: The nonlocal paradigm," *IEEE Signal Process. Mag.*, vol. 31, no. 4, pp. 69–78, Jul. 2014.

[21] A. Buades, B. Coll, and J.-M. Morel, "A review of image denoising algorithms, with a new one," *Multiscale Model. Simul.*, vol. 4, no. 2, pp. 490–530, 2005.

[22] C.-A. Deledalle, L. Denis, and F. Tupin, "How to compare noisy patches? Patch similarity beyond Gaussian noise," *Int. J. Comput. Vis.*, vol. 99, no. 1, pp. 86–102, 2012.

[23] D. La Torre, E. R. Vrscay, M. Ebrahimi, and M. F. Barnsley, "Measure-valued images, associated fractal transforms, and the affine self-similarity of images," *SIAM J. Imag. Sci.*, vol. 2, no. 2, pp. 470–507, 2009.

[24] T. Tasdizen, "Principal neighborhood dictionaries for nonlocal means image denoising," *IEEE Trans. Image Process.*, vol. 18, no. 12, pp. 2649–2660, Dec. 2009.

[25] J. Froment, "Parameter-free fast pixelwise non-local means denoising," *Image Process. On Line*, vol. 4, pp. 300–326, 2014.

[26] C.-A. Deledalle, L. Denis, and F. Tupin, "Iterative weighted maximum likelihood denoising with probabilistic patch-based weights," *IEEE Trans. Image Process.*, vol. 18, no. 12, pp. 2661–2672, Dec. 2009.

[27] C.-A. Deledalle, L. Denis, and F. Tupin, "NL-InSAR: Nonlocal interferogram estimation," *IEEE Trans. Geosci. Remote Sens.*, vol. 49, no. 4, pp. 1441–1452, Apr. 2011.

[28] K. Conradsen, A. A. Nielsen, J. Schou, and H. Skriver, "A test statistic in the complex wishart distribution and its application to change detection in polarimetric SAR data," *IEEE Trans. Geosci. Remote Sens.*, vol. 41, no. 1, pp. 4–19, Jan. 2003.

[29] G. Liu and H. Zhong, "Nonlocal means filter for polarimetric SAR data despeckling based on discriminative similarity measure," *IEEE Geosci. Remote Sens. Lett.*, vol. 11, no. 2, pp. 514–518, Feb. 2014.

[30] H. Feng, B. Hou, and M. Gong, "SAR image despeckling based on local homogeneous-region segmentation by using pixel-relativity measurement," *IEEE Trans. Geosci. Remote Sens.*, vol. 49, no. 7, pp. 2724–2737, Jul. 2011.

[31] H. Zhong, Y. Li, and L. Jiao, "SAR image despeckling using Bayesian nonlocal means filter with sigma preselection," *IEEE Geosci. Remote Sens. Lett.*, vol. 8, no. 4, pp. 809–813, Jul. 2011.

[32] S. Parrilli, M. Poderico, C. V. Angelino, and L. Verdoliva, "A nonlocal SAR image denoising algorithm based on LLMMSE wavelet shrinkage," *IEEE Trans. Geosci. Remote Sens.*, vol. 50, no. 2, pp. 606–616, Feb. 2012.

[33] S. Vitale, D. Cozzolino, G. Scarpa, L. Verdoliva, and G. Poggi, "Guided patchwise nonlocal SAR despeckling," *IEEE Trans. Geosci. Remote Sens.*, vol. 57, no. 9, pp. 6484–6498, Sep. 2019.

[34] H. Aghababaei, G. Ferraioli, S. Vitale, R. Zamani, G. Schirinzi, and V. Pascazio, "Nonlocal model-free denoising algorithm for single- and multichannel SAR data," *IEEE Trans. Geosci. Remote Sens.*, vol. 60, 2022, Art no. 5217315.

[35] R. C. Bilcu and M. Vehvilainen, "Fast nonlocal means for image denoising," *Digit. Photogr. III*, vol. 6502, 2007, Art. no. 65020R.

[36] R. Vignesh, B. T. Oh, and C.-C. J. Kuo, "Fast non-local means (NLM) computation with probabilistic early termination," *IEEE Signal Process. Lett.*, vol. 17, no. 3, pp. 277–280, Mar. 2010.

[37] V. Karnati, M. Uliyar, and S. Dey, "Fast non-local algorithm for image denoising," in *Proc. 16th IEEE Int. Conf. Image Process.*, 2009, pp. 3873–3876.

[38] J. Wang, Y. Guo, Y. Ying, Y. Liu, and Q. Peng, "Fast non-local algorithm for image denoising," in *Proc. Int. Conf. Image Process.*, 2006, pp. 1429–1432.

[39] D. Cozzolino, S. Parrilli, G. Scarpa, G. Poggi, and L. Verdoliva, "Fast adaptive nonlocal SAR despeckling," *IEEE Geosci. Remote Sens. Lett.*, vol. 11, no. 2, pp. 524–528, Feb. 2014.

[40] D. Liang, J. Ding, and Y. Zhang, "Efficient multisource remote sensing image matching using dominant orientation of gradient," *IEEE J. Sel. Topics Appl. Earth Observ. Remote Sens.*, vol. 14, pp. 2194–2205, 2021.

[41] C. Deledalle, "Probabilistic patch-based filter," Jan. 10, 2019. Accessed: Jul. 2021. [Online]. Available: https://www.charles-deledalle.fr/pages/ppb.php

[42] G. Poggi, "Image despeckling." Accessed: May 2020. [Online]. Available: https://www.grip.unina.it/research/86-sar-despeckling/86-fans.html

Dongxing Liang received the B.Eng. degree in electrical engineering in 2018 from Xidian University, Xi'an, China,, where he is currently working toward the Ph.D. degree in the area of radar image processing.
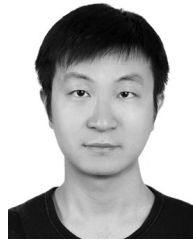
Ming Jiang received the B.Eng. degree in electronic engineering from Xidian University, Xi'an, China, in 2011, the M.Eng. and M.Res. degrees in image processing from IMT Atlantique, Rennes, France, in 2014, and the Ph.D. degree in astronomy and astrophysics from Université Paris-Sud, Orsay, France, in 2017.

From 2017 to 2020, he was a Postdoctoral Researcher with Signal Processing Laboratory 5, Swiss Federal Institute of Technology, Lausanne, Switzerland. He is currently an Assistant Professor with Xidian University. His research interests include computational imaging, optimization, and machine learning.

Jinshan Ding (Member, IEEE) received the B.Eng. degree from the Dalian University of Technology, Dalian, China, and the Ph.D. degree from Xidian University, Xi'an, China, both in electronic engineering.

From 2007 to 2014, he held a Research position with the Center for Sensor Systems, University Siegen, Siegen, Germany. He became an Associate Professor with Xidian University in 2014 and founded the Research Group of mm-wave and THz radar. He is currently a Chair Professor with the School of Electronic Engineering, Xidian University. His research interests include video synthetic aperture radar, distributed radar system, and radar signal processing algorithms.